RPE | Radiation Physics & Engineering
An International Peer-Reviewed Journal
Published by K.N. Toosi University of Technology
http://rpe.kntu.ac.ir
Research Article

Radiation Physics and Engineering 2022; 3(3):7–15
https://doi.org/10.22034/RPE.2022.334260.1058

Analysis and design of a 2.45 GHz RF power source for a miniature electron cyclotron resonance ion source

Hamid Rahimpour*, HamidReza Mirzaei, Masoomeh Yarmohammadi Satri
Physics and Accelerators Research School, NSTRI, P.O. Box 14395-836, Tehran, Iran

HIGHLIGHTS

- A solid-state RF power source is presented for the ECR ion source.
- A bias controller circuit is designed to protect the RF transistor.
- The proposed RF source can deliver up to 320 W power to the ion source chamber.

ABSTRACT

A high-power solid-sate based radio frequency power source is introduced in this paper. Solid-state based amplifiers are much more efficient than microwave tubes and can be used in compact electron cyclotron resonance (ECR) ion sources. A reliable negative bias voltage controller is proposed to drive the power source's main power amplifier, which can deliver up to 300 W power to the ion chamber. The selected high-power transistor is internally matched on the input side but the output side is matched in this paper to deliver maximum power to the load. The bias circuit was fabricated on an FR4 substrate and measurement results were obtained to verify the functionality of the bias sequencer. Analog simulations were done by LTSPICE and high-frequency simulations are performed with the momentum RF simulator of Advanced Design System (ADS). The output power of the proposed structure is tunable with 0.5 dB resolution and can deliver 300 mW to 300 W power to the ion chamber.

KEYWORDS

Solid-State
Power Amplifier
Microwave Tube
Accelerator
Ion Source

HISTORY

Received: 15 March 2022
Revised: 30 April 2022
Accepted: 9 May 2022
Published: Summer 2022

1 Introduction

Electron Cyclotron Resonance (ECR) ion sources are used to generate high intensity singly charged ions (Lapin et al., 2018). ECR ion sources can be divided into two categories: high-intensity and compact sources. Higher intensity ECR ion sources are used in accelerators and the compact size them are utilized in industry ion implantation (Latrasse et al., 2017; Tang et al., 2007; Wen et al., 2018; Xie, 1997). An RF (radio frequency) power source is applied to an ion source chamber with an electron cyclotron resonance frequency, obtained by the magnitude of the magnetic field. For compact ion sources, a medium radio frequency power range is selected to be applied to the ion chamber to use a permanent magnet and have a compact ion chamber (Bogomolov et al., 2019; Muramatsu et al., 2018).

Magnetron tubes are usually used as an RF source to be injected into the ion chamber (Grzebyk et al., 2018; Tanizuka, 1989). Magnetrons are a good choice for high power range but as they need high voltage bias and waveguide transmissions tubes, they are not efficient in compact size applications (ECR Ion Sources for Accelerators - INSPIRE n.d.) (Mathur et al., 2011; Takagi and Mori, 2000). On the other hand, they suffer from high power efficiency and lifetime. Recently solid-state based power sources are a good alternative for microwave tubes with the growth of the technology (Azizi et al., 2018; Dancila et al., 2017; Deo et al., 2018; Hazami, 2020; Luo et al., 2021; Soutehkeshan et al., 2020). Solid-state power amplifiers can be combined to deliver higher power to the load using power combiners (Candoré et al., 2010; Nemati et al., 2021). As a result, failures in one module of the power amplifier would not affect the total output power dramatically (Hoang, 2019; Piel et al., 2005). Although the output power of magnetrons can change in some ways solid-state amplifiers can deliver a wide range of the output power easily (Martin et al., 2001).

In the present work, a tunable solid-state power source is proposed which can tune the amount of output power

*Corresponding author: hrahimpour@aeoi.org.ir

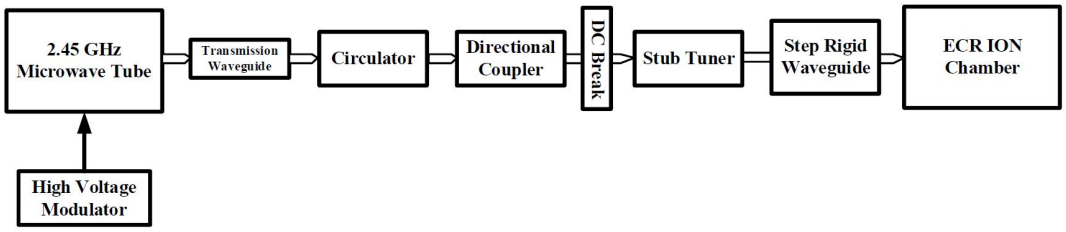

Figure 1: The Conventional block diagram of microwave tubes.

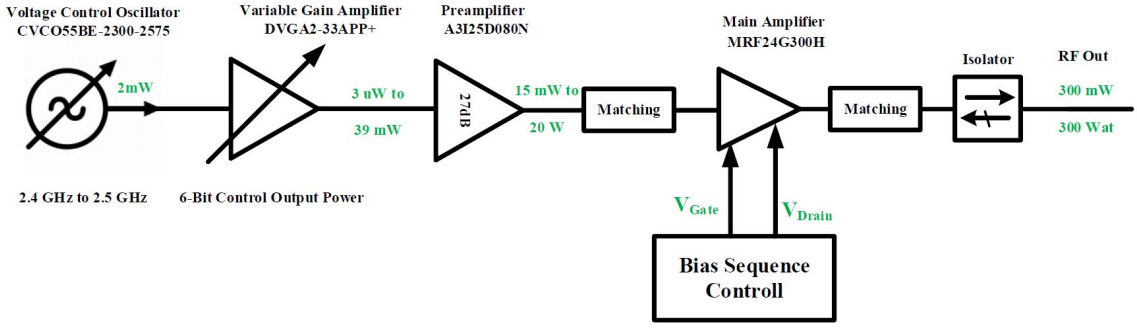

Figure 2: The Proposed Structure of Solid-State Power Source.

with 0.5 dB resolution and deliver it into the compact ECR ion source. The considered plasma chamber of the ion source has an equal length and diameter of 50 mm and is made of aluminum. For microwave propagation, the chamber length is selected larger than $\lambda/4$. A Gallium Nitride (GaN) power transistor is utilized as the main amplifier of the solid-state power source (MRF24G300HS, 2022). The selected transistor needs a negative gate voltage to work properly. As a result, a bias sequence should be considered to drive the transistor correctly. The bias circuit is a main controlling part of driving power amplifiers and avoids them from severe damage. Several works have been performed to increase the functionality of the bias circuit (Li et al., 2011; Yanjun et al., 2009; Tuo et al., 2009; Yang et al., 2018). A reliable bias sequence is designed and implemented in this paper to carefully protect the RF transistor which is the high-cost part of the solid-state power source.

This article is organized as follows. The conventional structure of microwave tubes is briefly described in Sec. 2. The proposed structure of the solid-state power source will be explained in Sec. 3. The suggested bias circuit is described in Sec. 4 and related results and discussions will be explained in Sec. 5. The article ends with conclusions and references.

2 The conventional structure of microwave tubes

The conventional block diagram of the microwave tubes is shown in Fig. 1. Generally, a magnetron is used as a power source in the frequency range of 2.45 GHz and power range about several hundreds of watts to tens of kilowatts (Muramatsu et al., 2018). A high voltage modulator is used to bias the magnetron and also an adaptor should be used to deliver the power from the tube to a proper waveguide like WR-340 (Lozovan et al., 2021). The output power will pass through several components like a circulator, directional coupler, stub tuner, and step rigid waveguide to meet the ion source chamber.

Occupied space, need for a high voltage modulator, low efficiency and a limited lifetime are the most important limitations of these structures. As a compact ion source is considered as a load of power source in this paper, a solid-state RF power source with a medium power range is much more suitable than a microwave tube. In the next section, the detailed procedure of designing a solid-state power source is explained.

3 The proposed structure of solid-state power source

The proposed structure of the solid-state based power source is depicted in Fig. 2. The proposed structure consists of a voltage-controlled oscillator, variable gain amplifier, preamplifier, main power amplifier, isolator, and bias sequence control. In the following, all parts of the proposed structure are explained in detail.

3.1 Voltage controlled oscillator

A voltage tunable oscillator with a frequency range of 2.3 to 2.57 GHz is used as a lowlevel RF source (Crystek, 2022). The output frequency will be set by changing the tuning voltage between 0.5 to 18V. The output power of the Voltage Controlled Oscillator (VCO) is about +2 dBm and its power consumption is less than 240 mW.

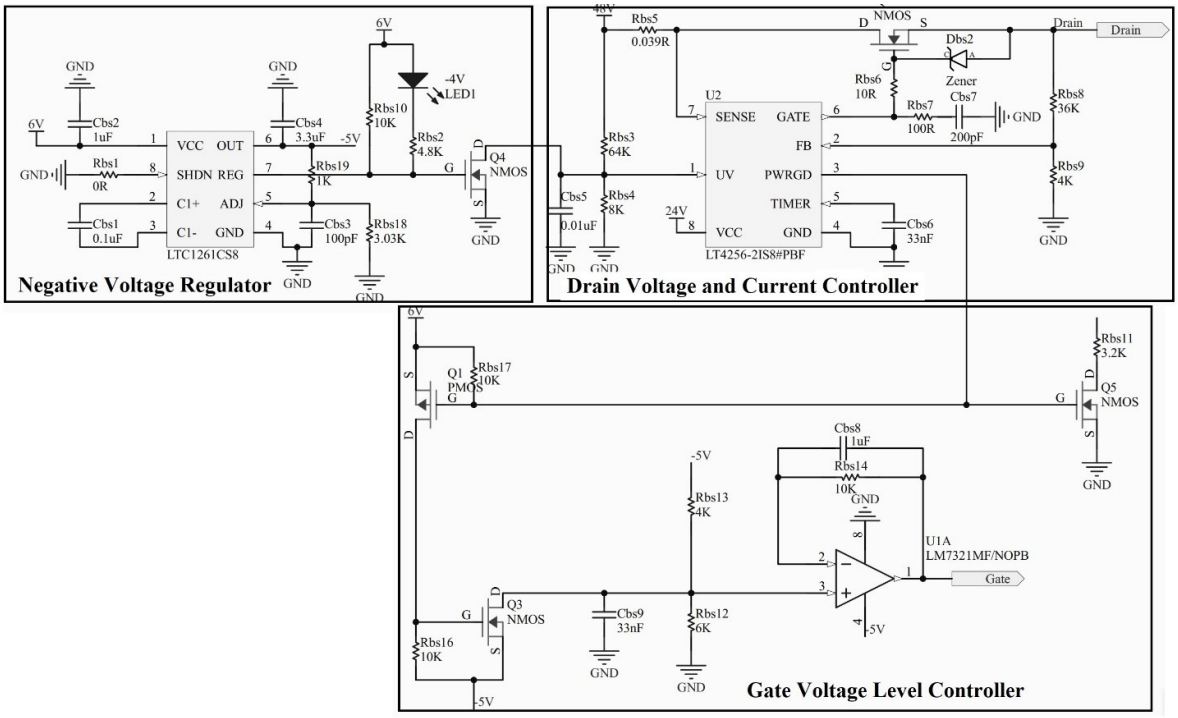

Figure 3: The Proposed Circuit of power amplifier bias sequence.

Table 1: The truth table of the variable gain amplifier control signals.

Attenuation (dB)	C_{16}	C_8	C_4	C_2	C_1	$C_{0.5}$
0	0	0	0	0	0	0
0.5	0	0	0	0	0	1
1	0	0	0	0	1	0
2	0	0	0	1	0	0
4	0	0	1	0	0	0
8	0	1	0	0	0	0
16	1	0	0	0	0	0
31.5	1	1	1	1	1	1

3.2 Variable gain amplifier

The output signal of the VCO is applied to a variable gain amplifier in Fig. 2. The utilized amplifier can change its output power from 3 uW to 40 mW (Mini-Circuits, 2022). This option is obtained by six control bits which are set by a digital value of '0' or '1'. Table 1. Shows the truth table of the several states of control bits. As the amplifier has a gain value of about 20 dB, the total gain of the Variable Gain Amplifier (VGA) can be changed from −11 to 20 dB.

3.3 Pre-amplifier

The main task of the preamplifier is to drive the main power amplifier. In the proposed structure at least 10 W power should be applied to the main power amplifier to obtain the maximum power of 320 W. As a result, a device is selected as a preamplifier in the proposed structure, to be able to deliver 20 W power to the main power amplifier. The selected preamplifier has about 27 dB power gain in the frequency range of 2300 to 2690 MHz (A3I25D080N, 2022).

3.4 Main power amplifier

The selected GaN-Based power transistor is one of the most efficient and high power amplifiers with a frequency range of 2.4 to 2.5 GHz which can deliver up to 320 W power to the ion source (MRF24G300HS, 2022). The drain voltage of the selected power amplifier should be 48V and it uses a negative gate voltage to work properly. The input of the power amplifier is almost internally matched but the output port is not matched and a matching network should be utilized. The transistor should have the bias sequence which will be explained in detail in the following section.

4 Bias sequencer design

A correct bias sequence with the following steps should be applied to the power transistor with negative gate voltage to work properly without any harmful damage that will be caused by unexpected over-current problems.
Turning the device ON:

1. Set VGS to -5 V
2. Turn on VD to the nominal supply voltage (48 V)
3. Increase VGS until desired drain current is attained
4. Apply RF input power to the desired level.

Turning the device OFF:

1. Turn RF power OFF

2. Reduce VGS down to -5 V
3. Reduce VD down to 0 V
4. Turn off VGS

Figure 3 shows the proposed circuit which can satisfy the mentioned sequence. We can divide the proposed circuit into three main parts consisting of a negative voltage regulator, drain voltage and current controller, and gate voltage level controller. We will explain these three parts in detail.

4.1 Negative voltage regulator

LTC1261 is used as a negative voltage regulator which can produce an adjustable negative voltage range from −1.25 to −8 V (LTC1261, 2022). Output negative voltage is adjusted by the value of R_{bs18} and R_{bs19} in Fig. 4 and has the following relation:

$$V_{bs} = -1.24 \times \frac{R_{bs18}}{R_{bs19}} \quad (1)$$

By choosing 3.03 kΩ and 1 kΩ for R_{bs18} and R_{bs19}, −5 V will be obtained by the regulator. The selected regulator has a 'REG' port which indicates whether the output voltage is settled or not. This port provides open collector output and when the output −5 V is stable, its value is pulled to a digitally low state. As a result, by the default state, the Q4 transistor in Fig. 4 is always ON and when the desired output voltage is settled at the output port, its state will change to OFF. We will use this port as a command signal to turn the drain controller ON.

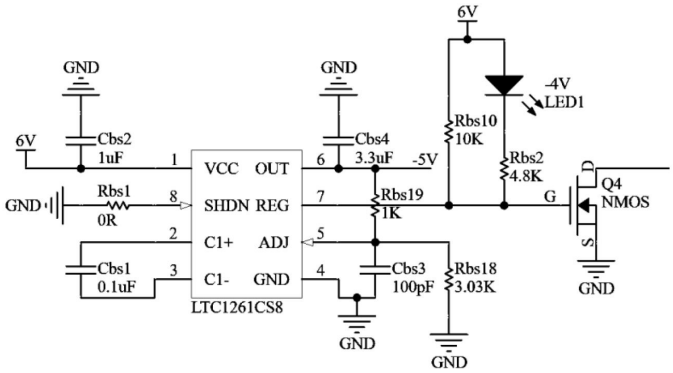

Figure 4: Negative Voltage Regulator part of the bias sequencer.

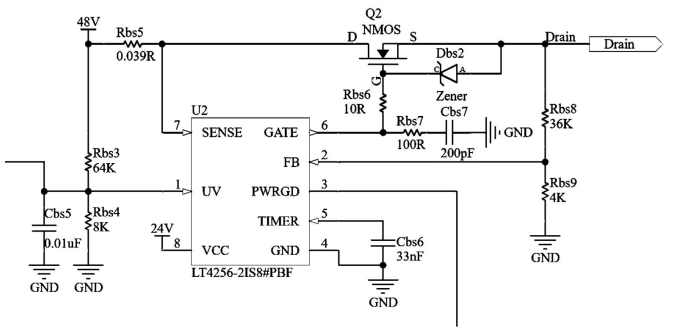

Figure 5: Drain controller part of the bias sequencer.

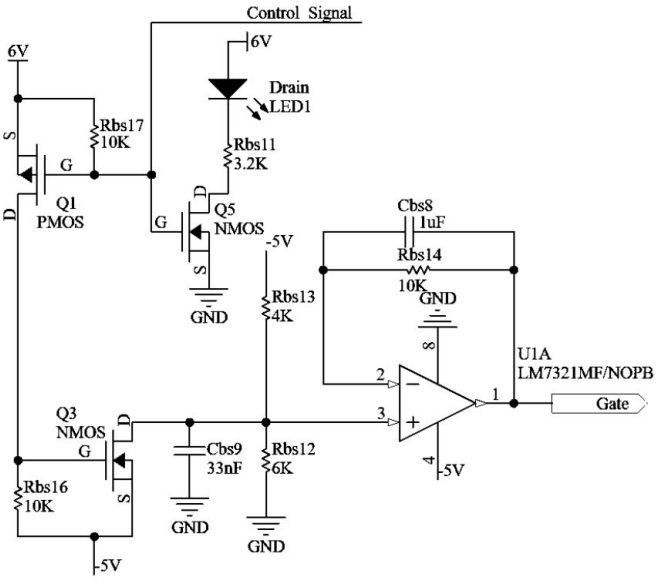

Figure 6: Gate voltage level controller.

4.2 Drain voltage and current controller

The circuit schematic of the drain controller is shown in Fig. 5. LT4256 is used as a drain hot-swap controller which can control both the drain voltage and current value (LT4256-1 and LT4256-2, 2022). When UV voltage on pin 1 exceeds 3.6 V, the controller will start working and the gate voltage of transistor Q2 in Fig. 5 will be charged. After a specified value, the transistor will be ON and 48 V will be connected to the Drain. In this situation the FB voltage will be calculated as follows:

$$V_{FB} = 48 \times \frac{R_{bs9}}{R_{bs9} + R_{bs8}} \quad (2)$$

When FB voltage exceeds 4 V, the PWRGD voltage on pin 3 changes its state from zero to open-collector state and can be used as a control signal of the gate voltage level.

4.3 Gate voltage level controller

Figure 6 shows the circuit schematic of the gate voltage level controller. The control signal of Fig. 6 comes from the drain controller PWRGD pin, and when the drain voltage is not applied this voltage will be zero and Q1 will be ON. Hence the gate voltage of Q3 is positive enough to turn it on. As a result, the drain voltage of Q3, which is the gate voltage of the main amplifier will be set to −5 V. So, whenever drain voltage is not applied, the gate voltage will be kept −5 V, which is one of the bias sequence steps. On the other hand, when the drain voltage is present at the output, the control signal will be open as a result Q1 and Q3 will be turned OFF and the gate voltage of the main power amplifier will be obtained as follows:

$$V_{Gate} = -5 \text{ V} \times \frac{R_{bs12}}{R_{bs12} + R_{bs13}} \quad (3)$$

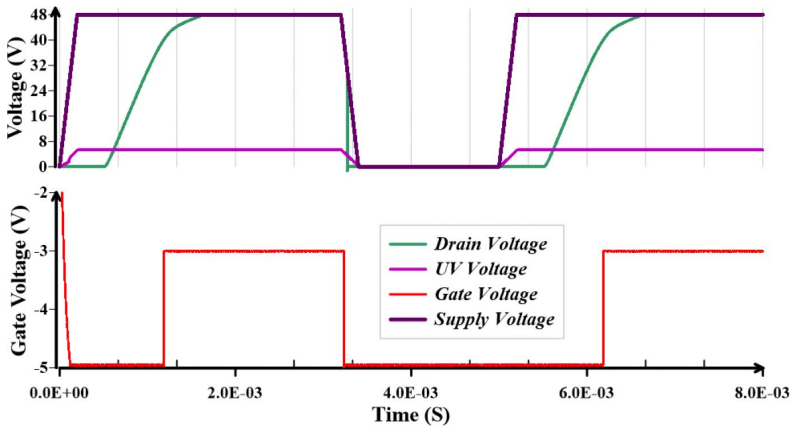

Figure 7: Voltage signals of the gate voltage level controller.

The values of these two resistors are selected so that after connecting the drain voltage, the gate voltage is equal to −3 V. The operational amplifier of Fig. 6 is added for buffering the final gate voltage so that the values of the selected resistors do not affect the gate input resistance.

By introducing the different parts of the proposed bias circuit, the overall performance of the bias sequence performance can be briefly described as follows. After applying a positive voltage to the bias circuit of Fig. 3, −5 V is generated by the mentioned regulator (and at the same time is applied to the gate voltage) then the REG voltage becomes zero and Q4 will be disconnected and the UV voltage starts charging to 5.33 V. After reaching the specified threshold value, the gate voltage of Q2 starts charging and turns it ON. When this transistor is turned on, the drain voltage will be connected to a 48 V. Consequently, the PWRGD signal becomes zero, Q1 and Q3 will be disconnected, and the gate voltage changes from −5 to −3 V.

As a result, according to the proposed bias circuit, the gate voltage changes (to −3 V) whenever 48 V is connected to the drain. Also, the drain voltage is connected to 48 V whenever −5 V is stable at the output of the regulator. This means that the first three conditions of the amplifier bias sequence are automatically met by the proposed circuit.

5 Results and discussion

Simulations have been done based on one measured scattering parameters model of the components of Fig. 2. All frequency-domain simulations have been performed by Advanced Design System (ADS). Matching network simulations also have been done based on the momentum radio frequency simulator of ADS and the exact parameters has imported into it. The high-frequency board substrate is Rogers RT6035HTC with 30 mil thickness. The bias circuit is simulated by LT-Spice and fabricated on a 1.6 mil FR4 substrate.

Figure 7 shows the drain and gate voltages of the bias controller circuit. Based on Fig. 7, when the supply voltage is applied, the UV voltage will be charged, and when reaches a higher voltage than 4 V, the gate of Q2 will be charged with $R_{bs7} \times C_{bs7}$ time constant. In this situation, the gate voltage will be kept at −5 V (red line in Fig. 7) until the drain voltage of Fig. 7 (green line) reaches more than a certain value, and the gate voltage will be changed to −3 V.

As was mentioned before, the main power transistor is only matched on the input side and it needs a matching network on the output side. Figure 8 shows the Printed Circuit Board (PCB) layout of the power amplifier with the matching network.

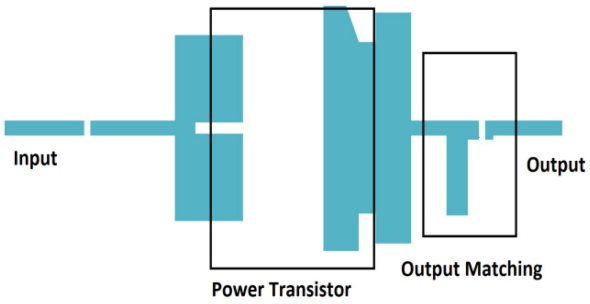

Figure 8: Layout of the power amplifier device with matching network.

Figure 9 demonstrates the frequency response of the power amplifier with and without a matching network. As it is shown the input and output return loss can be improved significantly based on the utilized matching network. Also, the center notch frequency of $S11$ and $S21$ can be tuned by changing the value of two capacitors on the output matching scheme. The effect of the matching network is also shown on the small-signal gain of the power amplifier. According to Fig. 10, the output matched amplifier has more than 25 dB power gain in comparison with the unmatched amplifier.

Another important parameter of the power amplifier is the isolation value which is shown in Fig. 11. According to this figure, the reflected power of the output port will be attenuated by more than 35 dB when passing through the power amplifier. It means that there is no need to use an isolator between the pre-amplifier and power amplifier.

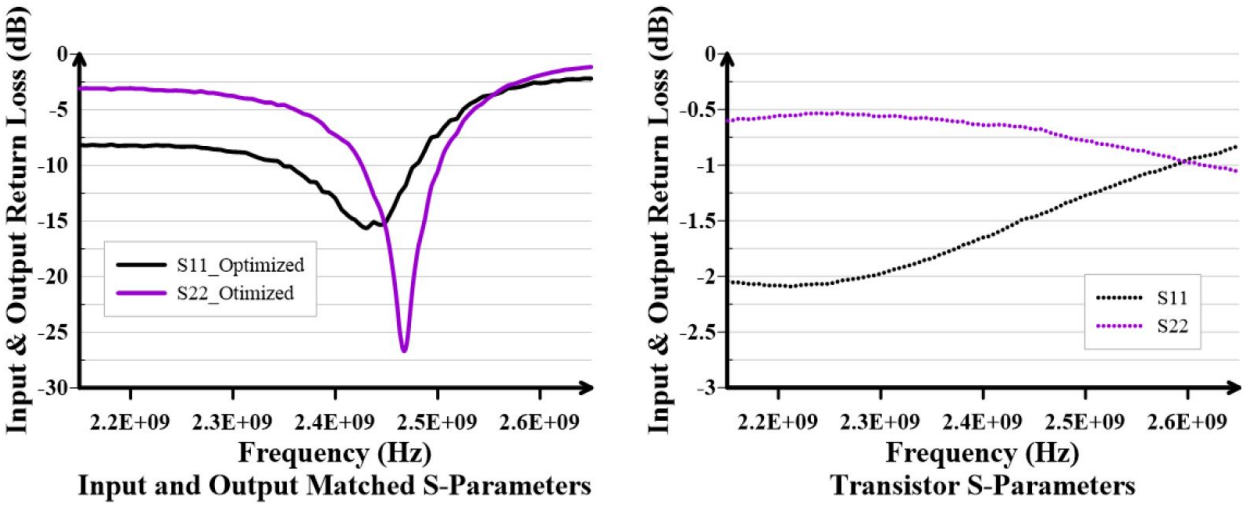

Figure 9: Frequency response of power amplifier with and without matching network.

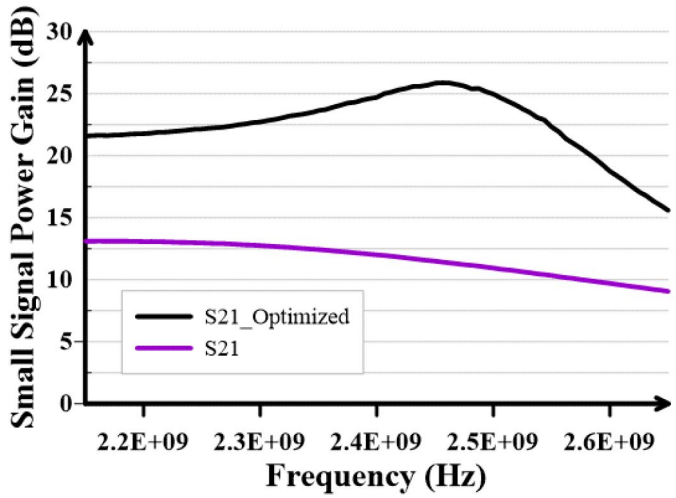

Figure 10: Power gain of the power amplifier with and without matching network.

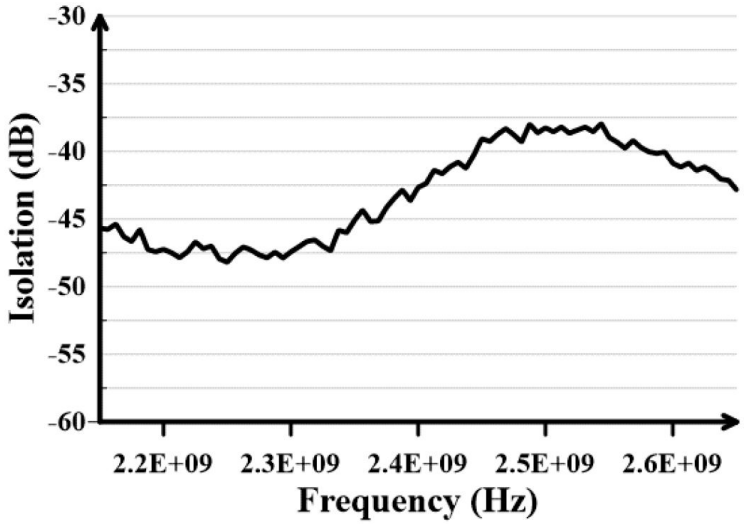

Figure 11: Isolation result of the power amplifier.

Table 2: Comparison of the proposed power source with other solid-state based works.

	Frequency (GHz)	Power (dBm)	Type Class	Efficiency (%)	Year
(Yang et al., 2015)	1.7-2.7	52.7-54.3	Doherty	<50	2015
(Chen et al., 2017)	2.7-3.1	<44	B	<44	2017
(Belaïd et al., 2020)	2.7-2.9	< 45	AB	<48	2020
(Cui et al., 2008)	1.99-2.01	<20	B	<70	2008
(Nakatani and Ishizaki, 2015)	2.4-2.5	50	F	<68	2015
Present Work	2.4-2.5	25-55	AB	<70	

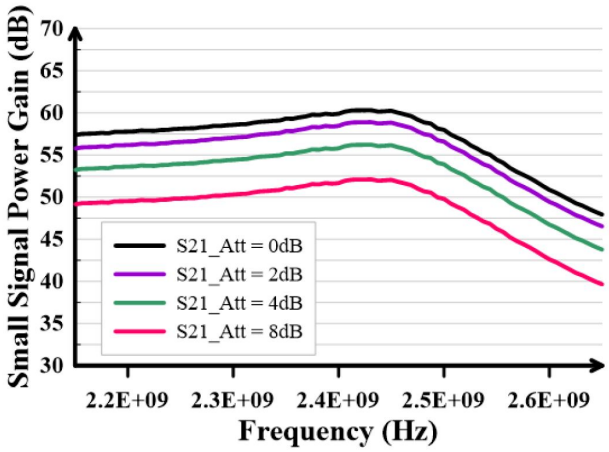

Figure 12: Small signal gain of the solid-state source.

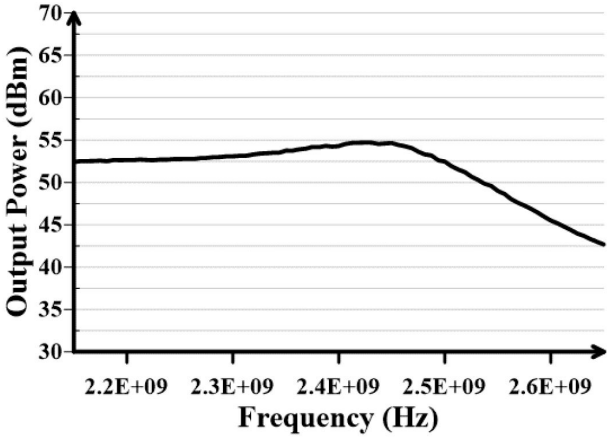

Figure 13: Isolation result of the power amplifier.

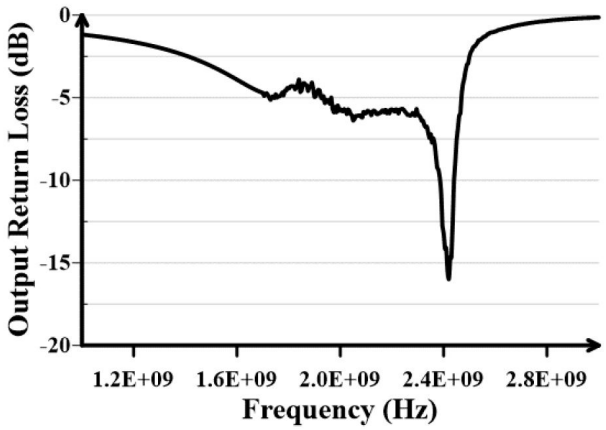

Figure 14: Output return loss of the solid-state source.

The total chain of the solid-state source in Fig. 2 is simulated based on measured scattering parameters of the utilized devices. Figure 12 shows the simulated small-signal gain of the total chain from VCO to the main power amplifier for different VGA attenuation values. The control bits of VGA help to fine-tune the output power with 0.5 dB resolution. The output power and return loss of the proposed solid-state source are depicted in Figs. 13 and 14, respectively. According to this figure, the maximum output power is about 55 dBm at the center frequency of 2.45 GHz and the output return loss is better than −15 dBm.

A comparison is made between the proposed power source with other related works and its result is shown in Table 2. All of the power sources in Table 2 are solid-state and work in S-band frequencies to have a fair comparison. According to the comparison table, the proposed power source has the most output power and power efficiency among others. The efficiency of the proposed power source is related to the power transistor directly and according to the device datasheet, it is more than 72%.

6 Conclusions

Design procedure of a solid-state gallium nitride power amplifier was shown in this paper. The proposed structure was designed at the center frequency of 2.45 GHz and can deliver up to 300 W power to the ion source chamber. As a compact ECR ion source is considered as a load, a solid-state power transistor was selected as a power source instead of a magnetron. Also, a reliable bias circuit was designed and implemented to drive the main power amplifier without failure and keep it safe from unwanted powering sequences. Simulations were performed to confirm the performance of the bias circuit before measurement results. Momentum-RF frequency-domain simulations have been done to show the output power of the solid-state source. Output power can be adjusted from 30 mW to 300 W with 0.5 dB resolution.

References

A3I25D080N (2022). A3I25D080N Product Information|NXP, https://www.nxp.com/part/A3I25D080N/ (March 14, 2022).

Azizi, H., Dehghan, M., Davani, F. A., et al. (2018). Design, construction and test of RF solid state power amplifier for IRANCYC-10. *Journal of Instrumentation*, 13(03):P03007.

Belaïd, M. A., Almusallam, A., and Masmoudi, M. (2020). Rf performance reliability of power N-LDMOS under pulsed-RF aging life test in radar application S-band. *IET Circuits, Devices & Systems*, 14(6):805–810.

Bogomolov, S., Bondarchenko, A., Efremov, A., et al. (2019). Development of compact 2.45 GHz ECR ion source for generation of singly charged ions. *Journal of Instrumentation*, 14(01):C01009.

Candoré, J. C., Bodnar, J. L., Detalle, V., et al. (2010). Non destructive testing in situ, of works of art by stimulated infrared thermography. In *Journal of Physics: Conference Series*, volume 214, page 012068. IOP Publishing.

Chen, X., Chen, W., Zhang, Q., et al. (2017). A 200 watt broadband continuous-mode doherty power amplifier for base-station applications. In *2017 IEEE MTT-S International Microwave Symposium (IMS)*, pages 1110–1113. IEEE.

Crystek (2022). https://www.crystek.com/home/vco/cvcodetail (March 14, 2022).

Cui, X., Doo, S. J., Roblin, P., et al. (2008). High efficiency RF power amplifier designed with harmonic real-time active load-pull. *IEEE Microwave and Wireless Components Letters*, 18(4):266–268.

Dancila, D., Duc, L. H., Jobs, M., et al. (2017). A compact 10 kW solid-state RF power amplifier at 352 MHz. In *Journal of Physics: Conference Series*, volume 874, page 012093. IOP Publishing.

Deo, R., Anghore, G., Jain, M., et al. (2018). Design and development of 3 kW pulsed solid-state RF power amplifier using two LDMOS in parallel configuration at 1 MHz. *Journal of Instrumentation*, 13(12):T12002.

Grzebyk, T., Szyszka, P., and Górecka-Drzazga, A. (2018). Magnetron-like miniature ion source. *Vacuum*, 151:167–174.

Hazami, Z. (2020). Development of a solid state amplifier for the 3^{rd} harmonic cavity for ALBA synchrotron light source.

Hoang, L. (2019). *High Power Radio Frequency Solid-State Amplifiers and Combiners for Particle Accelerators: From module to system design approach.* PhD thesis, Acta Universitatis Upsaliensis.

Lapin, R., Izotov, I., Skalyga, V., et al. (2018). Gasdynamic ecr ion source for negative ion production. *Journal of Instrumentation*, 13(12):C12007.

Latrasse, L., Radoiu, M., Nelis, T., et al. (2017). Self-matching plasma sources using 2.45 GHz solid-state generators: microwave design and operating performance. *Journal of Microwave Power and Electromagnetic Energy*, 51(4):237–258.

Li, C., Chen, Z., Huang, J., et al. (2011). An on-chip temperature compensation circuit for an InGaP/GaAs HBT RF power amplifier. *Journal of Semiconductors*, 32(3):035009.

Lozovan, A., Lenkovets, A., Ivanov, N., et al. (2021). Research of the influence of bias voltage on the structure and residual stress in Ta/W coatings applied on a copper substrate by inverted magnetron. In *Journal of Physics: Conference Series*, volume 2144, page 012012. IOP Publishing.

LT4256-1 and LT4256-2 (2022). LT4256-1 LT4256-2 Datasheet and Product Info | Analog Devices, https://www.analog.com/en/products/lt4256-1.html (March 14, 2022).

LTC1261 (2022). LTC1261 Datasheet and Product Info | Analog Devices. https://www.analog.com/en/products/ltc1261.html (March 14, 2022).

Luo, Y., Zhang, P., Lin, H., et al. (2021). Design and performance tests of a modular 166.6-MHz 50-kW compact solid-state power amplifier for the HEPS-TF project. *Journal of Instrumentation*, 16(04):P04011.

Martin, D., Jianu, A., and Ighigeanu, D. (2001). A method for the 2.45-GHz magnetron output power control. *IEEE Transactions on Microwave Theory and Techniques*, 49(3):542–545.

Mathur, Y., Rodrigues, G., Ahuja, R., et al. (2011). Design and development of a low cost 2.45 GHz ECR ion source for material sciences and other applications at IUAC, New Delhi. In *Proceedings of the DAE-BRNS Indian Particle Accelerator Conference*.

Mini-Circuits (2022). Mini-Circuits, https://www.minicircuits.com/WebStore/dashboard.html ?model=DVGA2-33APP

MRF24G300HS (2022). MRF24G300HS—300 W CW, 2400-2500 MHz, 50 V | NXP Semiconductors. https://www.nxp.com/products/radio-frequency/rf-industrial-scientific-and-medical/2450-mhz-ism/300-w-cw-over-2400-2500-mhz-50-v-rf-power-gan-transistor:MRF24G300HS (March 13, 2022).

Muramatsu, M., Kitagawa, A., Katagiri, K., et al. (2018). Optimization of Microwave Injection at Compact ECR Ion Source. In *2018 22nd International Conference on Ion Implantation Technology (IIT)*, pages 200–202. IEEE.

Nakatani, K. and Ishizaki, T. (2015). A 2.4 GHz-band 100 W GaN-HEMT high-efficiency power amplifier for microwave heating. *Journal of Electromagnetic Engineering and Science*, 15(2):82–88.

Nemati, R., Karimian, S., Shahi, H., et al. (2021). Multisection Combined Gysel–Wilkinson Power Divider With Arbitrary Power Division Ratios. *IEEE Transactions on Microwave Theory and Techniques*, 69(3):1567–1578.

Piel, C., Aminov, B., Borisov, A., et al. (2005). Development of a Solid State RF Amplifier in the KW Regime for Application with Low Beta Superconducting RF Cavities. In *Proceedings of the 2005 Particle Accelerator Conference*, pages 1–3. IEEE.

Soutehkeshan, A., Masoumi, N., and Alekajbaf, Y. (2020). A 10 Watts linear power amplifier using symmetric stub gando matching networks. In *2020 28th Iranian Conference on Electrical Engineering (ICEE)*, pages 1–6. IEEE.

Takagi, A. and Mori, Y. (2000). A 2.45 GHz microwave negative hydrogen ion source. *Review of Scientific Instruments*, 71(2):1042–1044.

Tang, D., Wang, L., Pu, S., et al. (2007). Characteristics of end hall ion source with magnetron hollow cathode discharge. *Nuclear Instruments and Methods in Physics Research Section B: Beam Interactions with Materials and Atoms*, 257(1-2):796–800.

Tanizuka, N. (1989). Analysis of magnetron ion sources and PIG ion sources. *Nuclear Instruments and Methods in Physics Research Section B: Beam Interactions with Materials and Atoms*, 37:189–193.

Tuo, W., Hongyi, C., and Dahong, Q. (2009). Theoretical analysis and an improvement method of the bias effect on the linearity of RF linear power amplifiers. *Journal of Semiconductors*, 30(5):055002.

Wen, J.-M., Peng, S.-X., Ren, H.-T., et al. (2018). A miniaturized 2.45 GHz ECR ion source at Peking University. *Chinese Physics B*, 27(5):055204.

Xie, Z. (1997). State of the art of ECR ion sources. In *Proceedings of the 1997 Particle Accelerator Conference (Cat. No. 97CH36167)*, volume 3, pages 2662–2666. IEEE.

Yang, S., Zhang, L., Fu, J., et al. (2018). On-chip bias circuit for W-band silicon–germanium power amplifier. *Journal of Semiconductors*, 39(12):125005.

Yang, Y., Zhang, M., Che, W., et al. (2015). High power S-band GaN-based power amplifier for radar systems. In *2015 IEEE MTT-S International Microwave Workshop Series on Advanced Materials and Processes for RF and THz Applications (IMWS-AMP)*, pages 1–3. IEEE.

Yanjun, P., Jiayou, S., Zhigong, W., et al. (2009). A 2.4-GHz SiGe HBT power amplifier with bias current controlling circuit. *Journal of Semiconductors*, 30(5):055008.